Original Article

INNOVATIVE CONTROL TECHNIQUES FOR ELECTRIC SPRINGS USING ACOQPCI

David Thompson

Department of Electrical and Computer Engineering, Texas A&M University, College Station, Texas, USA

Abstract: Electric Spring (ES) can effectively alleviate intermittent and instability issues in distributed power generation systems. However, the control effectiveness and response time are poor under traditional control methods, which severely impacts the regulation performance of the electric spring. To address the poor stability of the traditional proportional-integral controller applied to the electric spring system, this paper presents a control strategy based on Quasi-Proportional Complex Integral (QPCI) for the electric spring. By constructing the mathematical model of ES, designing the control strategy, and conducting stability analysis, the critical load voltage can quickly stabilize to the reference value. Furthermore, to address the issue of fixed parameters in the QPCI controller, an ant colony algorithm is introduced to adjust and optimize the parameters in real-time, thereby improving the system's dynamic response. Finally, the proposed control strategy is validated through Matlab/Simulink simulations, demonstrating that it can accurately and rapidly track the set value of the critical load voltage in the ES system, exhibiting strong adaptability and stability.

Keywords: Electric Spring, Voltage Fluctuation, Quasi-Proportional Complex Integral (QPCI).

1. Introduction

In recent years, the integration of large-scale renewable energy into the power grid has increased due to energy crisis and environmental concerns [1]. However, the intermittent and unpredictable nature of renewable energy results in power supply and demand imbalances [2], causing voltage and frequency fluctuations as well as harmonic pollution [3]. To address these issues, the first-generation Electric Spring (ES-1) was introduced [4,] providing reactive power compensation to stabilize critical load voltage. Compared to traditional demand-side management [5] and energy storage solutions [6], electric spring technology offers real-time and smooth control of load voltage during grid voltage fluctuations.

To enhance the performance of Electric Springs (ES), new ES topology structures and control strategies are continuously proposed and researched. Among them, a study discusses seven different ES topology structures [7], including ES-1 to ES-7. This paper focuses on ES-2, and current research efforts primarily concentrate on performance analysis and the development of control strategies. Various researchers have proposed different control schemes and optimization algorithms, such as phase control algorithms [8], the combination of Proportional Resonant controller with grid voltage feedforward [9,] fuzzy PI algorithms [10], and variable universe PI control algorithms [11]. The control strategies for ES are gradually evolving towards stronger robustness, nonlinearity, and intelligence.

Original Article

This paper proposes an electric spring control strategy based on the QPCI controller, and addresses the issues of traditional controllers using fixed parameter modes and poor dynamic performance in ES systems by optimizing them with the the Ant Colony Optimization (ACO). Firstly, the working principle and topology structure of ES are introduced and mathematically modeled. Secondly, based on this, a power spring control strategy based on QPCI is designed, and the stability of the system is verified using the Nyquist stability criterion. To address the fixed parameter issue, the ant colony optimization algorithm is introduced to dynamically adjust the optimal control parameters. Finally, the feasibility and effectiveness of the designed control strategy are verified by MATLAB/Simulink simulation.

2. ES Working Principle

The function of an Electric Spring (ES) system in a power system is similar to that of a vehicle shock Absorber, which can transfer voltage fluctuations to non-critical loads to stabilize the voltage of critical loads. Figure 1 shows a simplified single-phase ES system connection diagram, where the dashed line on the left represents a single-phase ES consisting of a single-phase voltage source inverter circuit and an LC filter. Z_{CL} is a critical load with a limited operating voltage range, while Z_{NCL} is a non-critical load with a wider operating voltage range. The ES is connected in series with Z_{NCL} to form a Smart Load (SL), which is connected in parallel with Z_{CL} to stabilize the voltage of critical loads. U_G represents the gridside voltage, and Z_{LINE} represents the impedance of the AC transmission line.
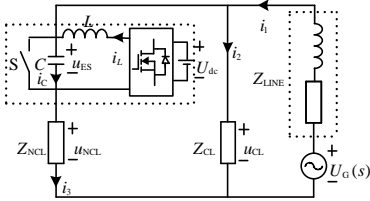

Figure 1: Single-phase ES system connection diagram.

If there is a voltage compensation requirement in the circuit, the control signal disconnects the switch S, and ES is connected in series with the non-critical load. The ES controller calculates the circuit quantity and generates a control signal that acts on the output compensation voltage of the inverter circuit, thereby stabilizing the voltage of the critical load. When ES is not involved in voltage compensation, S is closed and ES is shorted. According to the KVL principle, we can derive that:

$$u_{CL} = u_{ES} + u_{NCL} \quad (1)$$

Based on Equation (1), the phasor diagrams for the three operating modes of ES are shown in Figure 2. In these diagrams, $\dot{U}_{s\text{-ref}}$ represents the phasor of the reference voltage for the critical load, $\dot{U}_{SL}$ represents the phasor of the intelligent load voltage, and $\dot{U}_{ES}$ represents the phasor of the ES voltage. Figure 2(a) shows the resistive mode, where the terminal voltage of ES is zero when the grid operates at its rated state, that is, when $\dot{U}_{SL} = \dot{U}_{s\text{-ref}}$. Figure 2(b) shows the inductive mode, where ES generates an inductive voltage that leads the current by 90° to absorb reactive power from the bus as the grid voltage rises, thereby maintaining the voltage and power of the critical load. Figure 2(c) shows the capacitive mode, which operates on similar principles to the inductive mode.
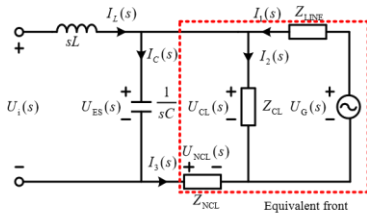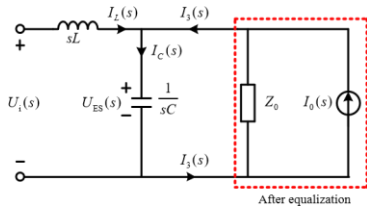
Original Article
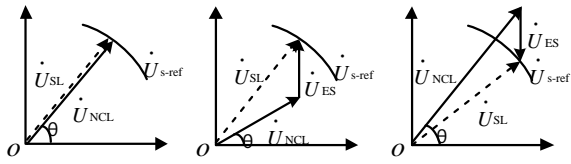
(a) Resistive mode   (b) Inductive mode   (c) Capacitive mode

Figure 2: Three working modes of ES.

Based on Figure 1, the s-domain model of the ES system is established in Figure 3:

(a) S-domain model of ES

(b) Equivalent S-domain model

Figure 3: S-domain circuit model of ES.

The expressions for the equivalent Z_0 and I_0 in Figure 3(b) are:

$$Z_0 = \frac{Z_{LINE}Z_{CL} + Z_{LINE}Z_{NCL} + Z_{CL}Z_{NCL}}{Z_{LINE} + Z_{CL}} \quad (2)$$

$$I_0(s) = U_G(s) \times \frac{Z_{CL}}{Z_{LINE}Z_{CL} + Z_{LINE}Z_{NCL} + Z_{CL}Z_{NCL}} \quad (3)$$

Based on the Norton equivalent principle, modeling of the ES system yields the s-domain expression for u_{CL} as:

$$U_{CL}(s) = G_1(s)U_i(s) G_2(s)U_G(s+) \quad (4)$$

While:

$$G_1(s) = \frac{Z_{LINE}Z_{CL}}{(Z_{LINE} + Z_{CL})(Z_0LCs^2 + Ls + Z_0)}$$

$$G_2(s) = \frac{Z_{CL}(Z_{NCL}LLCs + Ls^2 + Z_{NCL})}{(Z_{LINE} + Z_{CL})(Z_0LCs + Ls + Z_0)}$$

Original Article

Equation (4) indicates that ES is a dual-input single-output system, and the critical load voltage is affected by both the inverter output voltage $U_i(s)$ and the grid-side voltage $U_G(s)$. In practical control, $U_i(s)$ is considered as the controlled variable, while $U_G(s)$ is regarded as the disturbance variable.

3. Control Strategy Research

3.1. QPCI Control Principle

Compared to traditional PI control strategies, proportional complex integral (PCI) control can improve the control performance of AC systems and eliminate steady-state errors.

The transfer function of a traditional PI controller is:

$$G_{PI}(S) = K_P + \frac{K_i}{s} \quad (5)$$

For a PI controller, the gain of the DC component is:

$$G = \sqrt{K_P^2 + \left[\frac{K_i}{\omega_0}\right]^2} \quad (6)$$

The transfer function of a PCI controller is:

$$G_x(S) = K_P + \frac{K_i}{s - j\omega} \quad (7)$$

For a PCI controller, the gain of the controller at the AC angular frequency ω_0 is:

$$G = \sqrt{K_P^2 + \left[\frac{K_i}{0}\right]^2} \quad (8)$$

From the equation above, it can be seen that a PI controller can achieve zero steady-state error control for DC signals. However, at a given AC frequency ω_0, the controller has a limited gain, whereas a PCI controller has an infinite gain at the AC angular frequency ω_0. However, the PCI controller can only adjust the steady-state error of the AC component at the fundamental frequency, and adjusting it at other frequencies would cause a decrease in system gain. Therefore, introducing a QPCI controller with bandwidth ω_c can prevent the instability issue caused by infinite gain at the resonant frequency. Additionally, it can meet the requirements of steady-state error and improve the stability performance of the system. The transfer function of the QPCI controller is as follows:

$$G_x(s) = K_p + \frac{K_i\omega_c}{s - j\omega_0 + \omega_c} \quad (9)$$

In the control implementation, the transfer function of the RC phase shifter F(s)=(1-RCs)/(1+RCs) is utilized to simplify the control structure of the single-phase electric spring based on QPCI controller. It enables the realization of complex terms in the QPCI transfer function without the need for establishing a virtual coordinate system, thereby reducing the complexity of the control system. The block diagram of the QPCI control based on the RC phase shifter is shown in Figure 4, where RC is chosen as RC = $1/\omega_0$.
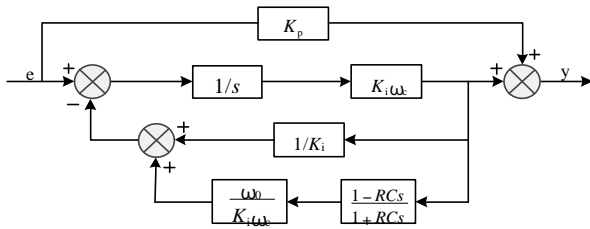
Original Article

Figure 4: QPCI control block diagram using all-pass filter.

3.2. ES Control Strategy Based On QPCI

The critical load voltage is influenced by both the inverter output voltage and the grid voltage, as can be seen from equation (4). In order to reduce the complexity of the control system and mitigate the influence of grid voltage disturbances, a control method incorporating grid voltage feedforward is introduced to better ensure the stability of the critical load voltage, as shown in Figure 5:
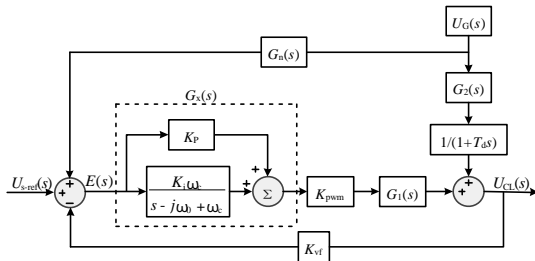

Figure 5: Block diagram of a feedforward control system.

Where K_{PWM} is U_{dc}/U_{tri}, representing the gain of the inverter. Taking into account the delay factor of the system, a small inertial component $1/(1+T_ds)$ is added after $G_2(s)$, where Td is half of the switching period T_s.

As shown in Figure 5, the transfer function of output voltage to grid voltage can be expressed as:

$$\frac{U_{CL}(s)}{U_G(s)} = \frac{G_2(s) + (1+T_ds)K_{PWM}G_1(s)G_n(s)G_x(s)}{(1+T_ds)[1+K_{PWM}G_1(s)G_x(s)]} \qquad (10)$$

In order to prevent the critical load voltage from being affected by the voltage on the grid side, the numerator of equation (10) is set to zero. At the same time, the expression for the feedforward transfer function $G_n(s)$ can be derived as:

$$G_n(s) = -\frac{G_2(s)}{(1+T_ds)K_{PWM}G_1(s)G_x(s)} \qquad (11)$$

By introducing the feedforward transfer function $G_n(s)$, the control system becomes a single-input single-output system influenced only by the inverter's output voltage, as shown in Figure 6.
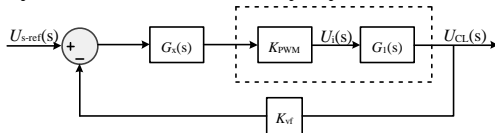

Figure 6: Simplified control system block diagram.

Original Article

From Figure 6, we can obtain the open-loop transfer function of the simplified system without the controller, which is:

$$G_o(s) = K_{PWM}G_1(s) \qquad (12)$$

The simplified system can be analyzed using the Nyquist stability criterion to determine the stability of the closed-loop system. The system parameters are shown in Table 1:

Table 1: System parameter setting table.

Parameter	Numerical value
DC side voltage U_{dc}/V	480
Carrier amplitude U_{tri}/V	1
Transmission line resistance R_1/Ω	0.6
transmission line inductance L_1/ mH	2.86
Critical load R_{CL}/Ω	40
Noncritical load R_{NCL}/Ω	4
Low pass filter inductance L/ mH	3.6
Low-pass filter capacitance C/μF	100
Voltage feedback coefficient K_{vf}	1
Current feedback coefficient K_{if}	0.754

Substituting the system parameters in Table 1 into equation (12), we obtain the expression for the denominator of the transfer function $G_o(s)$ as fifth-order, and the numerator as third-order. The calculation difficulty is relatively high. Therefore, the zero-pole cancellation method is adopted to simplify $G_o(s)$ to $G_{eq}(s)$:

$$G_{eq}(s) = \frac{4.5806\times10^9 s + 3.2342\times10^{11}}{s^3 + 1421s^2 + 9.459\times10^6 s + 1.045\times10^{10}} \qquad (13)$$

Multiplying the transfer function $G_x(s)$ of the QPCI controller by $G_{eq}(s)$, we obtain the open-loop transfer function $G_v(s)$ of the system with the controller, which is:

$$G_v(s) = G_x(s)G_{eq}(s) \qquad (14)$$

If the closed-loop system is stable, then the difference between the number of positive and negative crossings of the Nyquist plot on the real axis (-1, -∞) and half of the number of open-loop poles in the right half of the real axis is equal. This stability criterion is expressed as equation (15):

$$N_+ - N_- = \frac{P}{} \qquad (15)$$

In the equation, N_+ represents the number of times the Nyquist curve crosses the real axis (-1, -∞) from top to bottom, N_- represents the number of times it crosses the real axis (-1, -∞) from bottom to top, and P represents the number of open-loop poles in the right half of the s-plane.

Draw the pole-zero plot of $G_v(s)$ and the Nyquist curve of the system by substituting the parameters in Table 1 into equation (15). Set K_p and K_i to 5 and 50, respectively, with ω_0 as 314 rad/s and ω_c as 3.14 rad/s, as shown in Figures 7 and 8.
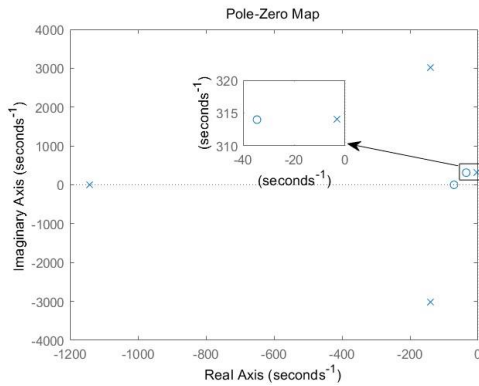
Original Article
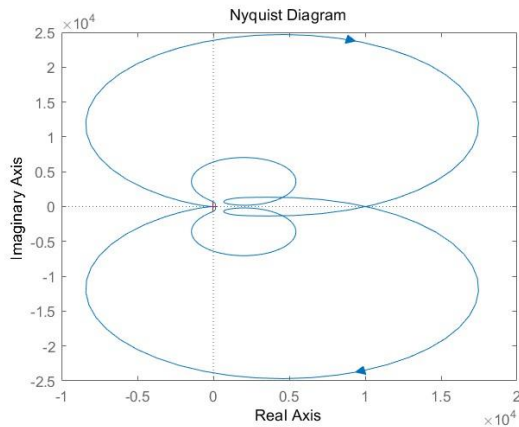

Figure 7: Pole zero distribution map.

Figure 8: System Nyquist curve.

From Figure 7, it can be observed that all four poles of the open-loop transfer function $G_v(s)$ lie in the left-half plane of the s-plane, indicating a P-value of 0. Furthermore, based on Figure 8, the Nyquist curve of the open-loop system does not cross the real axis (-1, -∞) in either direction, with a crossing count of 0. Combining this information with equation (15), it can be concluded that the system is Table. 3.

4.   Parameter Optimization Based on Ant Colony Algorithm

The design objective of the electric spring system is to ensure stability and fast regulation of the critical load voltage. However, due to its time-varying and nonlinear characteristics, using fixed parameter values would degrade the system's dynamic performance. The K_p and K_i parameters of the QPCI controller affect system stability and response speed, and they are typically adjusted empirically. Therefore, in this paper, an ant colony optimization is used to iteratively optimize the K_p and K_i parameters of the controller, aiming to improve the system's dynamic performance.

4.1.   Basic Principle of Ant Colony Algorithm

The ant colony algorithm is based on simulating the behavior of ants searching for food paths, which transforms the problem of finding the optimal solution into a problem of finding the optimal path[12]. During the search process, ants continuously release pheromones and search for paths under the guidance of pheromones. When an ant finds a better path, it releases more pheromones to attract other ants to follow the same path[13]. Through

Original Article

repeated iterations, the concentration of pheromones gradually increases, and eventually all ants converge on the path to the global optimal solution. In this article, the probability formula for ants to select a specified path is as follows: Basic Principle of Ant Colony Algorithm

$$P_{ij}k(t) = \frac{[\tau_{ij}(t)]^\alpha [\eta_{ij}(t)]^\beta}{\sum [\tau_{is}(t)]_\alpha [\eta_{is}(t)]_\beta} \quad j,s \in allowed\ k \quad (16)$$

□ S∈allowed k

□ 0 ,others

Where 'allowed k' refers to the feasible points for ants, $\tau_{ij}(t)$ represents the concentration of pheromones between points i and j, and $\eta_{ij}(t)$ is the heuristic function between i and j, which can be expressed as $\eta_{ij}(t)=1/distance(i,j)$. α is the pheromone heuristic factor. β plays a critical role in the convergence of the algorithm.

After completing one iteration of the search process, the ant colony algorithm updates the pheromone levels between the currently selected paths to improve the overall performance of the algorithm. The update rule is as follows:

$$\tau_{ij}(t+1)=(1-\rho)_{ij}(\tau t)+\Delta\tau_{ij}(t)$$

$$\Delta\tau_{ij}(t)=\sum_{k=1}^{n} {}_{ij}\Delta\tau^{k}(t) \quad (17)$$

Here ρ represents the pheromone evaporation rate, $\Delta\tau_{ij}$ represents the sum of all pheromones released by the ants on the path, and $\Delta\tau_{ij}{}^k$ represents the pheromone level released by the k-th ant on the path between i and j.

4.2. **Parameter Optimization of Ant Colony Algorithm**

Ant colony algorithm regards the proportional and integral parameters of the QPCI controller as paths in the search space. Ants choose paths based on the concentration of pheromones. With each iteration of the search, the concentration of pheromones gradually increases, and eventually all ants will converge to the globally optimal path. In this way, the ant colony algorithm can find the optimal control parameters to achieve the optimization of control system performance

To achieve the optimal selection of control parameters, this study employs the ant colony algorithm and designs corresponding performance indicators to evaluate its performance in solving combinatorial optimization problems. In the traditional traveling salesman problem ⁽TSP⁾ [15], the evaluation criterion is based on the shortest distance of the path crossing all target points. Inspired by this, the study uses the integral of absolute error as a performance indicator to evaluate the control performance of the QPCI controller. Since the rise time, overshoot, and settling time are important performance indicators for evaluating the QPCI controller's performance, the integral of absolute error is used to approximate the overall deviation between the expected output and the actual output, as shown in equation (18).

$$Q = T^2 \sum_{i=1}^{LP} i\ |e(i)| \quad (18)$$

In summary, the steps for optimizing the QPCI controller using the ant colony algorithm are as follows:

Original Article

▪   Initialize the ant colony and parameters: set the number of ants, initial value of pheromones, constant transfer probability, maximum iteration times, and other parameters;

▪   Record the path points of ants and place them in a matrix;

▪   The algorithm iterates, and the colony starts at the origin. Formula (16) is used to calculate the transfer probability, select the next node, and record the current ant node into the matrix;

▪   When an iteration is completed, calculate the corresponding control parameters and performance indicators for each ant's path matrix. Update the pheromones according to equation (17), and record the minimum performance indicator and corresponding control parameters for this iteration;

▪   If the algorithm has not converged and the maximum iteration times have not been reached, start the next iteration; otherwise, output the convergence result or the current optimal result as the optimal parameter solution.

5.   Simulation Verification

Build an ES system simulation model in MATLAB/Simulink, using the system parameters in Table 1 for simulation. Validate the effectiveness of the ACO-QPCI control strategy proposed in the article when there is a temporary voltage rise or drop in the power grid.

Specifically, when the power grid voltage U_G is 262V, the critical load voltage is 220V. Set the simulation to control signal S to disconnect at 0.03s, activate the power spring, and simulate voltage fluctuations of +15% and -15% by setting U_G to 301.3V and 222.7V, respectively, to simulate temporary voltage rise and drop in the power grid. The simulation time is 0.5s, and the voltage U_G varies over time as shown in Table 2.

Table 2: Variation of voltage UG over time.

Time	U_G/V
0-0.1	262
0.1-0.25	222.7
0.25-0.35	262
0.35-0.5	301.3

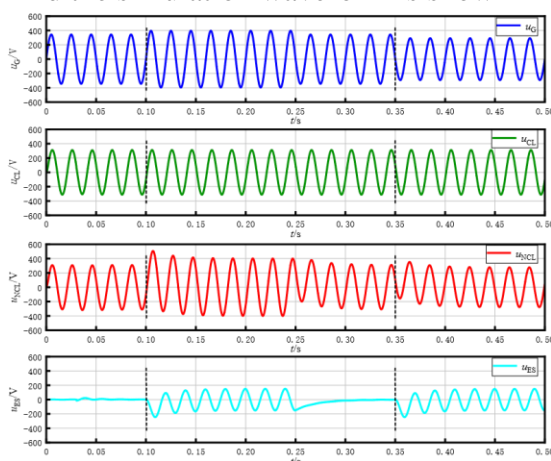And the simulation waveform is shown in Figure 9:

Figure 9: Simulation diagram using the proposed control strategy.

From the simulation results in Figure 9, the following observations can be made:

Original Article

▪ From 0.1s to 0.25s, the grid voltage is higher than the reference value. During this period, U_{ES} lags behind U_{NCL}, and the ES operates in the capacitive mode. It injects negative reactive power into the grid to stabilize the voltage at the terminals of the critical load.

▪ From 0.25s to 0.35s, the grid voltage matches the reference value. The power spring operates in the resistive mode, and the voltage values at the non-critical load and critical load are essentially the same. However, due to additional voltage effects on the output filter of the ES, the voltage at the terminals of the power spring is not exactly zero.

▪ From 0.35s to 0.45s, the grid voltage exceeds the reference value. During this period, U_{ES} leads U_{NCL}, and the power spring operates in the inductive mode. It injects positive reactive power into the grid to stabilize the voltage at the terminals of the critical load. These observations confirm the correctness of the adopted control strategy.

To validate the advantages of the ACO-QPCI controller proposed in this article in terms of fast tracking, a Proportional-Integral (PI) controller was used for comparison. The simulation parameters for the comparison with the PI controller were manually tuned based on experience, with $K_p = 5$ and $K_i = 10$.
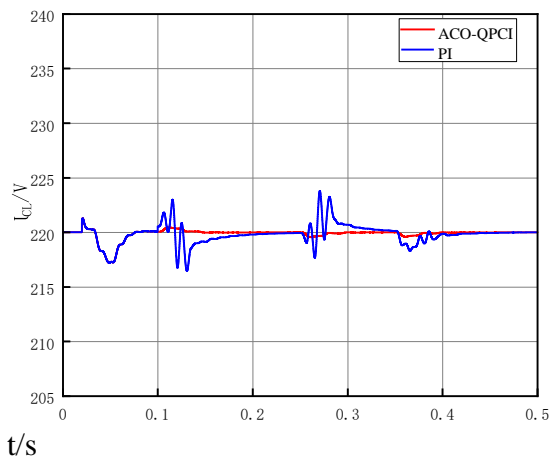

t/s

Figure 10: Variation of effective value of uCL when uG fluctuates.

At 0.03s, the ES acts on the circuit, causing a slight fluctuation in the rms value of u_{CL}. However, it quickly stabilizes at the reference value. From the graph, it can be observed that the PI control strategy exhibits a large overshoot, with u_{CL} voltage fluctuating by approximately 8V when u_G fluctuates. Additionally, the adjustment period is long, taking 0.1s to return to a stable state, which is not conducive to the operation of the critical load. In contrast, the ACO-QPCI control strategy shows better performance. When u_G fluctuates, it controls u_{CL} voltage to fluctuate by no more than 1V, and it can recover to a stable state within 0.05s. Its control performance is significantly superior to that of the PI controller.

With the simulation parameters unchanged, the sensitivity of the ACO-QPCI control strategy is tested when there is a sudden change in the non-critical load. In the simulation, the power supply voltage u_G remains constant at 262V. At 0.3s, when the non-critical load is switched from 100 Ω to 50 Ω, the amplitude and rms value of u_{CL} change, as shown in the following graph.

Original Article
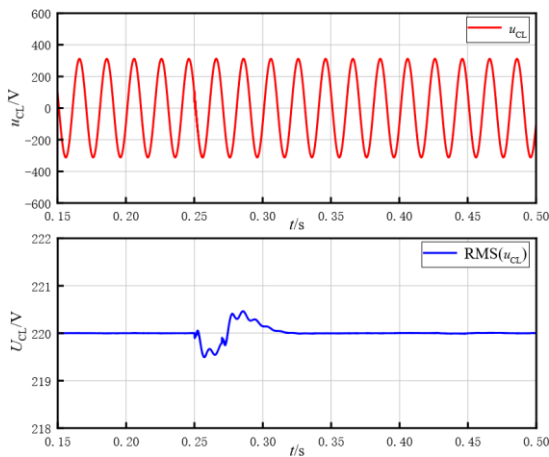

Figure 11: Changes in u_CL when switching non-critical loads.

From Figure 11, it can be seen that at 0.3 seconds, the transient disturbance caused by the switching of non-critical loads results in a temporary voltage fluctuation of the critical load, with an amplitude not exceeding 1 V. However, the fluctuation in the RMS (root mean square) value is small and returns to a stable state within 0.05 seconds. Therefore, it can be concluded that the ACO-QPCI control strategy has a minimal impact on the voltage of critical loads during non-critical load mutations, and it can quickly stabilize to the desired value.

6.   Conclusions

To address the issue of poor dynamic adjustment performance in traditional ES controllers, the paper investigates the ES topology and related control strategies. It proposes a power spring control strategy based on ACO-QPCI and validates it through Matlab/Simulink simulations. The results indicate the following:

(1)   The control strategy effectively transfers grid voltage fluctuations to non-critical loads and utilizes ES voltage compensation to maintain the critical load at the desired reference state.

(2)   During grid voltage fluctuations, the ES can stabilize the voltage of the critical load within two fundamental frequency cycles. Compared to the PI control strategy, it exhibits smaller overshoot and better speed.

(3)   When switching non-critical loads, the proposed control strategy can quickly stabilize the voltage of the critical loads to the ideal state and effectively improve the robustness of the system.

References

Hossein S, Hesam M, Hossein R, et al. Utilization of in-pipe hydropower renewable energy technology and energy storage systems in mountainous distribution networks [J]. Renewable Energy, 2021, 172.

S. Geethanjali, S. Shanmugapriya, Niket, et al. Electric Springs with Management of Battery in Order to Reduce Voltage Fluctuations [J]. International Journal of Recent Technology and Engineering (IJRTE), 2019, 8(2s11).

Mohamed F, Ahmed I. O, Israa M. M, et al. Strategies to save energy in the context of the energy crisis: a review [J]. Environmental Chemistry Letters, 2023, 21(4).

Hui S Y R, Lee C K, Wu F. Electric springs: a new smart grid technology [J]. IEEE Transactions on Smart Grid, 2012, 3 (3): 1552-1561.

Original Article

A. J. Roscoe and G. Ault, Supporting high penetrations of renewable generation via implementation of real-time electricity pricing and demand response, IET Renewable Power Generation, vol. 4, no. 4, pp. 369–382, Jul. 2010 A. Mohd, E. Ortjohann, and A. Schmelter, Challenges in integrating distributed energy storage systems into future smart grid, IEEE Symposium on Industrial Electronics, pp. 1627-1632, 2008. [7] Yin F G, Wang C. Analysis of the effective operating range of electric spring based on reactive power compensation [J]. Power System Protection and Control, 2019, 43(01): 174-184.

Wang Q S, Cheng M, Chen Z, Wang Z. Steady-State Analysis of Electric Springs With a Novel delta Control [J]. IEEE Transactions on Power Electronics, 2015, 30(12).

Cheng M, Wang Q S, Zhang J Z. Theoretical Analysis and Controller Design of Electric Springs [J]. Proceedings of the CSEE, 2015, 35(10): 2436-2444.

Wu J, Wang B H. Design of an electric spring controller based on optimal PI [J]. Electrical Automation, 2017, 39(04):39-43.

Xuan M H, Zhang J H, Wang S J, et al. Electric spring control strategy based on variable universe fuzzy PI control [J]. Science Technology and Engineering, 2020, 20(18):6.

Meng X, Zhu X, Zhao J. Obstacle avoidance path planning using the elite ant colony algorithm for parameter optimization of unmanned aerial vehicles [J]. Arabian Journal for Science and Engineering, 2023, 48(2): 2261-2275.

Lina H. The global path planning for vehicular communication using ant colony algorithm in emerging wireless cloud computing [J]. Wireless Networks, 2022, 29(2).

Kang Y F, Li Z B, Wang T. Application of PaID Control and Improved Ant Colony Algorithm in Path Planning of Substation Inspection Robot [J]. Mathematical Problems in Engineering, 2022, 2022.

Riabko A V , Zaika O V , Kukharchuk R P, et al. Algorithm of ant colony optimization (ACO) for 3D variation traveling salesman problem[J]. Journal of Physics: Conference Series, 2022, 2288(1).